6. Vortex lattice methods

1. Review of vortex filaments

Vortex filaments are lines in 3D space around which flow circulates. They are governed by Helmholtz theorems:

(1) Vortex filaments do not end in the fluid – they may end on a solid surface, extend to infinity or form closed loops.
(2) They have constant circulation along their length.

The line vortex studied earlier was an example of a vortex filament, extending to $\pm\infty$ in the direction perpendicular to the page. In a plane perpendicular to any vortex filament the flow close to the line will look like the flow around a line vortex. Vortex filaments are classed as singularity solutions of 3D potential flow in the same way as line sources and line vortices were singularity solutions of 2D flow; the flow satisfies Laplace's equation everywhere except on the filament itself, on which the velocity is infinite.

The classic application to aircraft aerodynamics (Figure 1) is to consider the whole aircraft and trailing vortex system as modelled by a single vortex filament known as a horseshoe vortex. The bound vortex follows the wing aerodynamic centre and connects to two trailing vortices extending to infinity behind the aircraft. The starting vortices shed every time the aircraft changes its lift can be considered as effectively closing a vortex loop downstream. If these are sufficiently far downstream they can be ignored so far as computing the aircraft aerodynamics is concerned.

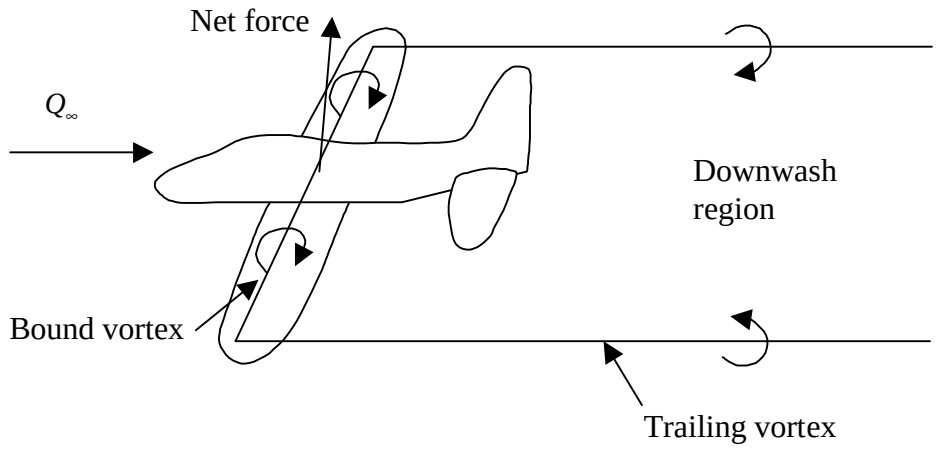

Figure 1.Basic horseshoe vortex model of an aircraft.

The velocity field associated with a vortex filament is given by the Biot-Savart law, which was originally derived to solve the analogous electro-magnetic problem of computing the magnetic field around a current-carrying wire. For our purposes we only need the integrated Biot-Savart result for a straight line segment AB of a vortex filament (Figure2; see chapter appendix 1 for a derivation).

The velocity at point C is perpendicular to the triangle ABC with magnitude given by

$$\boxed{w = \frac{\Gamma}{4\pi h}\left(\cos\theta_A - \cos\theta_B\right)} \qquad (1)$$

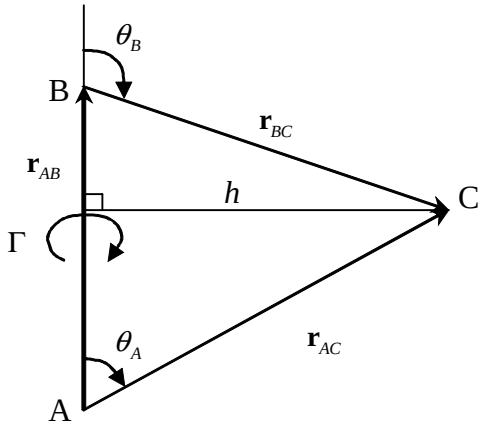

Figure 2. Geometry to illustrate the velocity at point C due to a segment AB of a vortex filament.

where *h* is the perpendicular distance between point C and the line tangent to AB. The direction of *w* for positive circulation is given by a right hand rule (with thumb pointed along the segment from A to B, the curled fingers give the velocity direction). So long as the aircraft wing is planar this equation can be used as is. However for other configurations it will be useful to have a more general version. Suppose A, B and C are general points in 3D space and let the sides of the triangle ABC be vectors $\mathbf{r}_{AB}$, $\mathbf{r}_{AC}$ and $\mathbf{r}_{BC}$. By the cosine rule we have

$$\mathbf{r}_{AB}\bullet\mathbf{r}_{AC} = r_{AB}r_{AC}\cos\theta_A$$
$$\mathbf{r}_{AB}\bullet\mathbf{r}_{BC} = r_{AB}r_{BC}\cos\theta_B$$

where a bold typeface denotes a vector and an italic its magnitude. Substituting into (1) and using the cross product of r_{AC} and r_{BC} normalised by its magnitude to give the direction of the resulting velocity we have the vector velocity **w** as

$$\mathbf{w} = \frac{\Gamma}{4\pi h}\frac{\mathbf{r}_{AC}\times\mathbf{r}_{BC}}{\left|\mathbf{r}_{AC}\times\mathbf{r}_{BC}\right|}\left(\frac{\mathbf{r}_{AB}\bullet\mathbf{r}_{AC}}{r_{AB}r_{AC}} - \frac{\mathbf{r}_{AB}\bullet\mathbf{r}_{BC}}{r_{AB}r_{BC}}\right)$$

We also need the perpendicular distance *h*, which can be obtained by recognising that the area hr_{AB} is equal to the parallelogram area $\left|\mathbf{r}_{AC}\times\mathbf{r}_{BC}\right|$. Thus finally

$$\boxed{\mathbf{w} = \frac{\Gamma}{4\pi}\frac{\mathbf{r}_{AC}\times\mathbf{r}_{BC}}{\left|\mathbf{r}_{AC}\times\mathbf{r}_{BC}\right|^2}\mathbf{r}_{AB}\bullet\left(\frac{\mathbf{r}_{AC}}{r_{AC}} - \frac{\mathbf{r}_{BC}}{r_{BC}}\right)} \qquad (2)$$

Equation (2) is a cornerstone of all vortex filament methods, so it is worth writing it into a small function *vfil*, to be called from various programs in the remainder of this Chapter.

A segment of a vortex filament held fixed in a velocity field will experience a force according to the Kutta-Joukowski theorem. (Again we have an analogy with the force on a current-carrying wire in a magnetic field.) The direction of the force is normal to the plane containing the relative velocity and the vortex segment and can be found by a right-hand rule (first finger in direction of velocity **q**, second finger in direction of vortex filament $\mathbf{r}_{AB}$, and thumb gives the direction of the force). To get the direction mathematically we take the cross product of the velocity and the direction of the vortex segment, leading to a 3D filament version of the Kutta-Joukowski theorem

$$\boxed{\mathbf{F} = \rho\Gamma\mathbf{q}\times\mathbf{r}_{AB}} \qquad (3)$$

In equations (1) or (2) and (3) we have the nuts and bolts of vortex lattice theory. The basic methodology from now on is the same as for the lumped vortex model in 2D.

```
function[l] = vfil(xa,xb,xc)

% Inputs are the x,y and z co-ordinates of three points in space.
% The function works out the influence of vortex line AB at control point C,
returning zero if the
% denominator is less than 'small', so that self-influences are excluded.

small = 1.0e-12
ab = xb-xa;
ac = xc-xa;
bc = xc-xb;
cross = [ac(2)*bc(3)-ac(3)*bc(2); ac(3)*bc(1)-ac(1)*bc(3); ac(1)*bc(2)-
ac(2)*bc(1)];
den = 4.0*pi*(cross(1)^2 + cross(2)^2 + cross(3)^2);
absac = sqrt(ac(1)^2 + ac(2)^2 + ac(3)^2);
absbc = sqrt(bc(1)^2 + bc(2)^2 + bc(3)^2);
num = ab(1)*(ac(1)/absac-bc(1)/absbc) + ab(2)*(ac(2)/absac-
bc(2)/absbc) + ab(3)*(ac(3)/absac-bc(3)/absbc);
if den< =small
    l = [0.0;0.0;0.0];
else
    l = num/den*cross;
end
```

Program 1. Influence of a straight line vortex segment AB on a control point C in general 3D space.

2. Single horseshoe vortex model of a wing

The component of the freesteam velocity normal to the wing must match the summed normal components due to all the segments of the horseshoe vortex at some defined control points. In 2D we fixed the control point so that the lift slope matched the thin aerofoil result. In 3D we have two free parameters: the chordwise location of the control point and the distance between the trailing vortices. We can choose these to satisfy any sensible conditions we like. A useful form arises when we choose them to match the 2D thin aerofoil lift slope result ($a_w = 2\pi$) for high aspect ratio wings and the slender wing result ($a_w = \pi AR/2$) for low values of the aspect ratio.

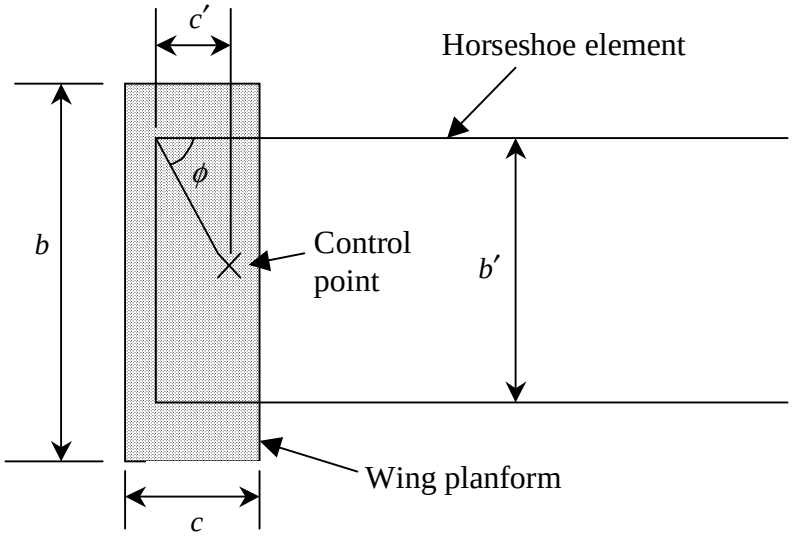

Figure 3. Single element model of a rectangular wing.

The angle ϕ (which will be related to the wing aspect ratio) is defined by

$$\tan\phi = \frac{b'}{2c'} \tag{4}$$

The influences of the bound and trailing vortices can be found by writing θ_A and θ_B in terms of ϕ. For small incidences we have

$$w = \frac{\Gamma}{4\pi}\left[\frac{1}{c'}\left(\cos\left(\tfrac{\pi}{2}-\phi\right)-\cos\left(\tfrac{\pi}{2}+\phi\right)\right)+\frac{2}{b'}\left(1-\cos\left(\pi-\phi\right)\right)+\frac{2}{b'}\left(\cos\phi+1\right)\right],$$

where the three terms inside the square brackets correspond to the contributions from AB, $A'A$ and BB' respectively. This simplifies to

$$w = \frac{\Gamma}{2\pi}\left[\frac{\sin\phi}{c'}+\frac{2}{b'}\left(1+\cos\phi\right)\right] \tag{5}$$

The basic equation is for tangential flow at the control point i.e. $w = U_\infty \alpha$. Since $L = \rho U_\infty \Gamma b'$ we can write down the wing lift coefficient as

$$C_L = \frac{L}{\frac{1}{2}\rho U_\infty^2 bc} = \frac{2\Gamma b'}{U_\infty bc}$$

Combining with (5) and differentiating with respect to incidence we have an expression for the wing lift slope

$$a_w = 4\pi\frac{b'c'}{bc}\frac{1}{\sin\phi+2\frac{c'}{b'}\left(1+\cos\phi\right)} \tag{6}$$

For small aspect ratios $\phi \to 0$ $\sin\phi \to 0$ and $\cos\phi \to 1$, leaving

$$a_w = \pi AR\left(\frac{b'}{b}\right)^2$$

If we want to recover the slender wing result $a_w = \pi AR/2$ we see that we have to choose $b' = b/\sqrt{2}$. For large aspect ratios $\sin\phi \to 1$ and we can drop the second term in the denominator of (6), leaving

$$a_w = 4\pi\frac{b'c'}{bc}$$

Now we will recover the thin aerofoil result $a_w = 2\pi$ if we choose $c' = c/\sqrt{2}$.

Substituting these values back into (6) gives the lift slope of a wing for any aspect ratio

$$\boxed{a_w = \frac{2\pi AR}{AR\sin\phi+2\left(1+\cos\phi\right)}} \tag{7}$$

where ϕ is related to the aspect ratio from (4) by $\tan\phi = AR/2$.

Figure 3a shows the variation of lift slope with aspect ratio from this formula. This confirms that at low aspect ratios one recovers the slender wing result, while lift slope increases monotonically thereafter.

A few lines of algebra shows that this result is identical to the Helmbold equation

$$a_w = \frac{2\pi}{\left[1+\left(\frac{2}{AR}\right)^2\right]^{1/2}+\frac{2}{AR}}$$

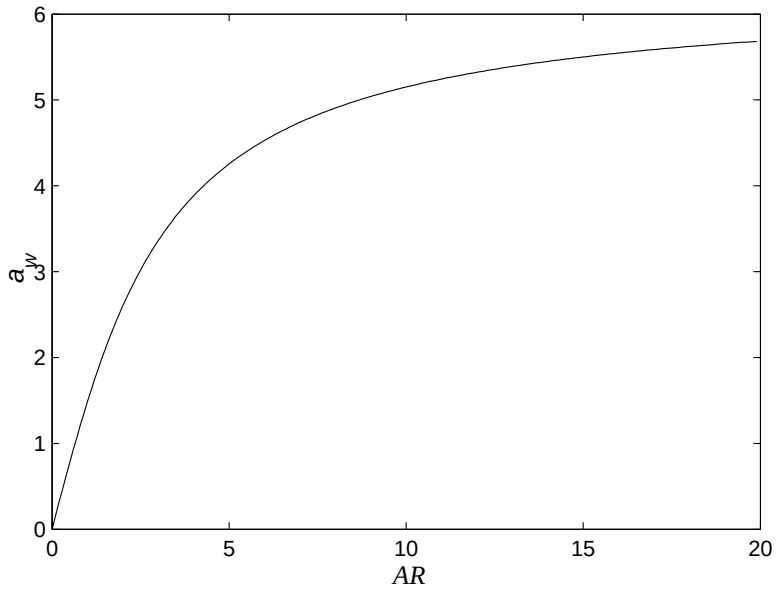

Figure 3a. The effect of aspect ratio on wing lift slope according to the single horseshoe element model of a wing.

with $a_\infty = 2\pi$. For large values of *AR* this reduces to the standard result of lifting line theory for elliptic planforms

$$a_w = \frac{2\pi}{1+\frac{2}{AR}}$$

Thus the single horseshoe vortex model with a distance between the trailing vortices of $b' = b/\sqrt{2}$ and a control point for tangential flow located a distance $c' = c/\sqrt{2}$ behind the wing aerodynamic centre is sufficient to reproduce the lift slope of both slender wing theory and lifting line theory for elliptic planforms.

The induced drag can also be computed. At a load point located at the centre of the bound vortex $\phi = \pi/2$ and the downwash velocity due to the two trailing vortices is

$$w = \frac{\Gamma}{\pi b'} = \frac{C_L U_\infty}{\pi AR}$$

The lift force acts normal to the velocity at the load point, as shown in the sketch below

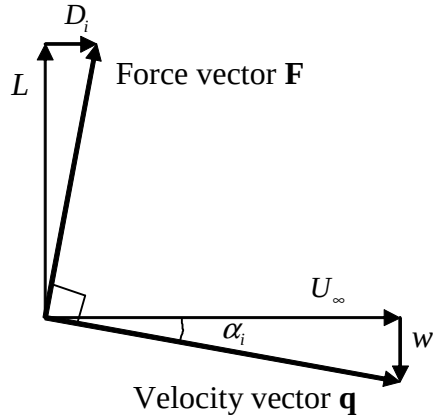

Figure 4. Local velocity and force at the load point.

For small angles, the induced angle of attack is $\alpha_i = w/U_\infty$ and the induced drag coefficient is

$$\boxed{C_{D_i} = \frac{C_L^2}{\pi AR}} \tag{8}$$

This is one of the most important results of aerodynamics, identifying the aspect ratio as the dominant parameter controlling the lift-dependent drag: to reduce the induced drag of planar wings one needs to increase the aspect ratio. Again, this result is the same as that derivable from lifting line theory of elliptic planforms. Clearly this simple model has a lot going for it and in the next section we extend the method towards a more complete wing analysis tool.

3. *N*-element horseshoe vortex model

The extension to *N*-elements follows in the same way as the lumped vortex model was extended. In the standard method *N* horseshoe vortex elements are arranged across the span of the wing, with bound elements on the quarter-chord line and control points at the three-quarter chord position. However this standard model will not produce all the nice results of the previous section when we use $N = 1$. To overcome this we set the span coverage of the elements, b', and the locations of the control points, c', behind the quarter chord line to be

$$b' = b\sqrt{\frac{N}{N+1}} \tag{9a}$$

and

$$c' = \frac{c}{2}\sqrt{\frac{N+1}{N}} \tag{9b}$$

For $N = 1$ we reduce to the expressions of the previous section, recovering the results for an elliptic planform or a slender wing, while for large *N* we have elements that span the whole wing with control points tending to the three-quarter chord position. The overall arrangement is shown on Figure 6 below for four elements.

To set up the matrix elements we need the influence of the *j*'th horseshoe vortex on the *i*'th control point. Then we add up the influences of all the vortices and impose the tangential flow condition. The geometry of each interaction is sketched on Figure 7. The locations of each of the points are known from Figure 6, so all that is needed to get the influence of the horseshoe vortex is to add up the three contributing parts: i.e. (following the filament around) $A'A$, AB and BB', where the points A' and B' are located a long way downstream behind *A* and *B* respectively. For a planar wing such as shown this can be accomplished easily using equation (1). However, for later application to non-planar wings we prefer to invoke the function *vfil*, which is good for any orientation of the three points. Also keeping generality in mind, we do not make the assumption of small angles and instead store a surface normal vector **n** for each control point. If the free stream velocity vector is denoted by $\mathbf{Q}_\infty$, the flow normal to the surface due to the freestream is $\mathbf{Q}_\infty \cdot \mathbf{n}_i$. The boundary condition to be solved is of zero normal velocity at each control point i.e.

$$\sum_{j=1}^{N} \Gamma_i \left(\mathbf{I}_{AA'} + \mathbf{I}_{AB} + \mathbf{I}_{BB'} \right)_{ij} \cdot \mathbf{n}_i = -\mathbf{Q}_\infty \cdot \mathbf{n}_i \tag{10a}$$

or in final matrix form

$$\mathbf{A\Gamma} = \mathbf{R} \tag{10b}$$

where **A** is an *N* by *N* matrix, $\mathbf{\Gamma}$ is the required solution vector, and **R** is the known right hand side vector.

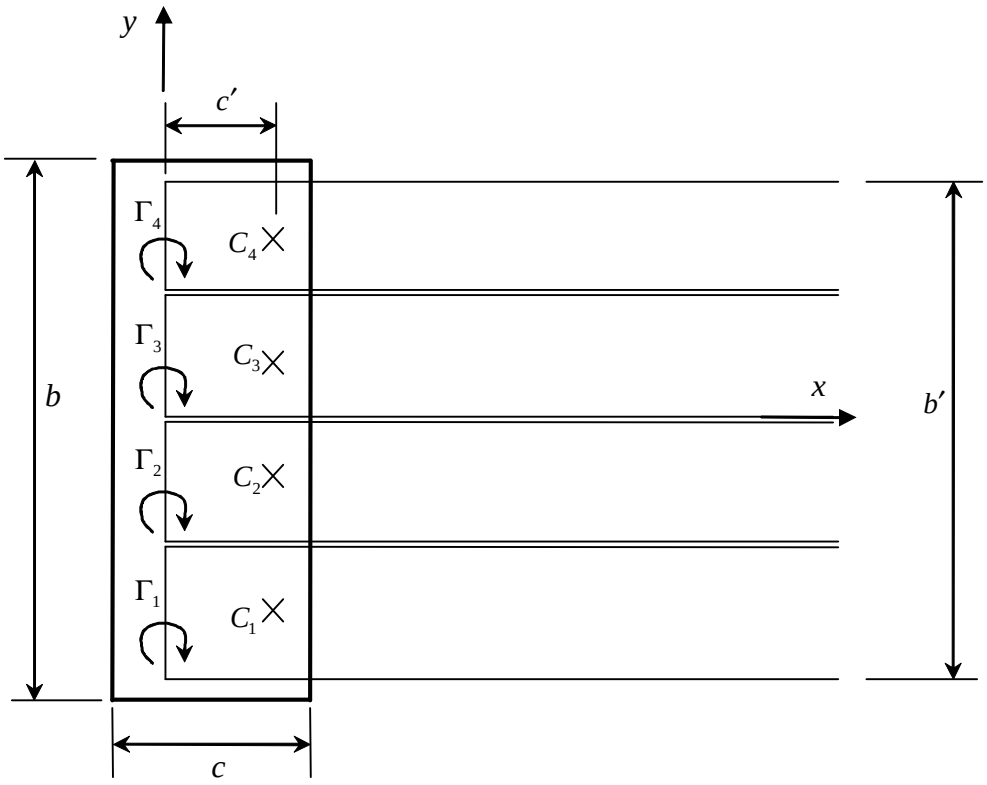

Figure 6. General arrangement of horseshoe elements for a four element model of a rectangular wing planform. The gaps between the trailing vortices are for illustration only: in reality the elements are overlaid.

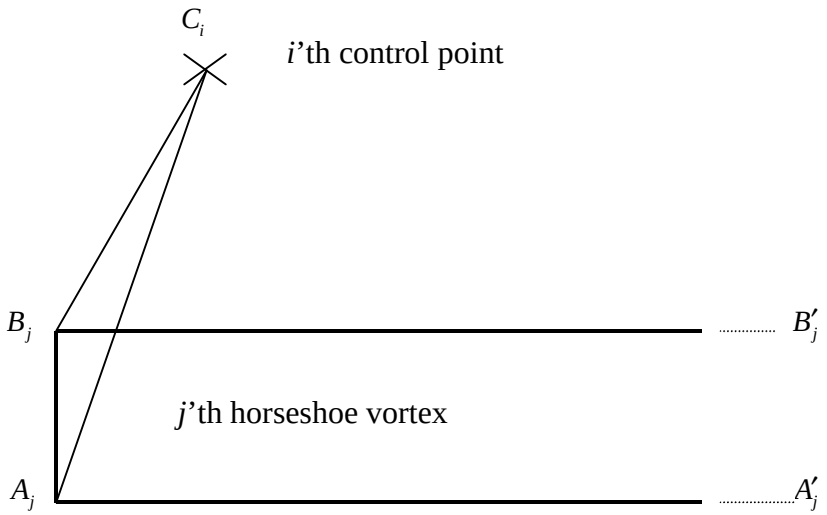

Figure 7. Influence of the *j*'th horseshoe vortex on the *i*'th control point.

The program *wing* below illustrates the procedure. Inputs to the program are the wing incidence (the angle of the zero lift line relative to the free stream), the aspect ratio, and the number of elements to use. The program is in three parts

1. The geometry is set up and the co-ordinates of the points A and B for each horseshoe element are found, together with the locations of all the control points C.
2. The influence matrix and right hand side vector are set up. This involves three calls to *vfil* for each segment of the horseshoe vortex. Adding up the vector influences and taking the dot

product with the normal vector gives us the influence coefficients, which are stored in the matrix **A**. At the same time we compute the right hand side vector.

3. After solving the system of equations, we need to do some more work to compute the forces, which are given by (3) as normal to the plane containing each bound vortex filament and its local velocity. The local velocity at the centre of each bound vortex is found by adding all the influences. Then the vector (cross) product gives the components of the resultant force vector on each element. Finally these are all added together and converted to lift and drag coefficients. Recall that lift is always measured normal to $\mathbf{Q}_\infty$ and drag parallel to it.

The convergence of the method, for a rectangular wing with aspect ratio equal to 4, is shown on figure 8, compared with the results of the same methodology, but with the horseshoe elements filling the span of the wing and the control points always at the three-quarter chord position. Both methods converge to the same result, but the method presented here is better behaved for small *N*, matching smoothly to the elliptic planform result.

The effect of aspect ratio on a rectangular wing is shown on Figure 9 for calculations with $N = 100$. The top graph compares the lift slope to Helmbold's equation, while the lower plots the induced drag factor

$$\delta = C_{D_i} \pi AR / C_L^2 - 1 \qquad (11)$$

which would be zero for en elliptic distribution of circulation. Rectangular wings clearly generate less lift and more drag for a given incidence and aspect ratio than elliptic wings for the same wing aspect ratio.

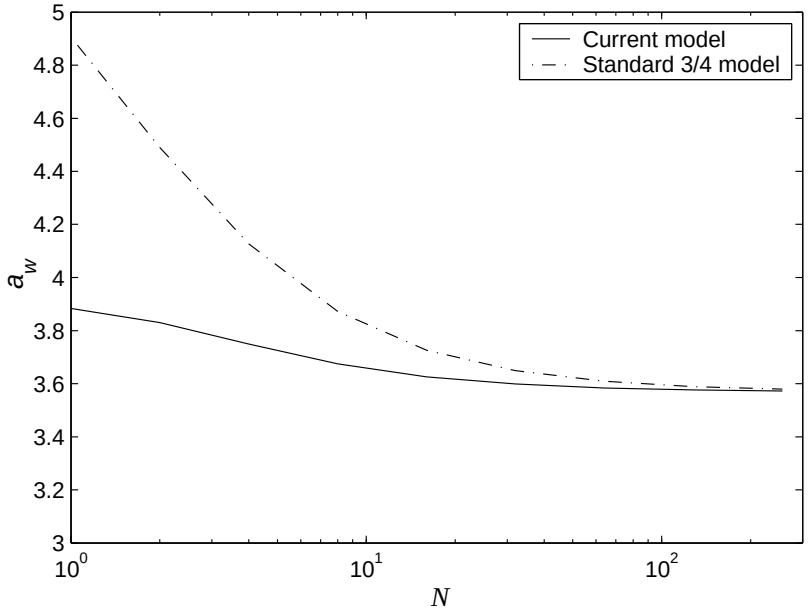

Figure 8. Convergence of the *N*-element horseshoe vortex model for the lift slope of a rectangular wing of aspect ratio 4. In the current model span and control point locations are defined by (9), while in the standard model the elements span the entire wing and the control points are always at the three-quarter chord position.

```
function[Cl,Cd] = rectwing(alpha,AR,N)

% outputs: lift and drag coefficients
% inputs: incidence alpha (relative to zero lift line), aspect ratio AR and number of elements N

large = 1.0e6;                          %length of the trailing vortices
Q = [cos(alpha); 0.0; sin(alpha)];      %velocity (relative to the zero lift line)
bw = AR;    cw = 1.0;                   %wing data
fact = sqrt(N/(N + 1));                 % horseshoe vortex sizes (according to N-element model)
bp = bw*fact;    cp = 0.5*cw/fact;

%locations of vortex segments, control and normal vectors
dy = bp/N;
xa(:,1) = [0.0;-0.5*bp;0.0];
xb(:,1) = [0.0;-0.5*bp + dy;0.0];
for i = 2:N
    xa(:,i) = xb(:,i-1);
    xb(:,i) = xa(:,i) + [0.0;dy;0.0];
end
for i = 1:N
    xc(:,i) = 0.5*(xa(:,i) + xb(:,i)) + [cp;0;0];
    n(:,i) = [0.0;0.0;1.0];
end

%set matrix and right hand side elements and solve for circulations
for i = 1:N
    for j = 1:N
        I = vfil(xa(:,j),xb(:,j),xc(:,i));
        I = I + vfil(xa(:,j) + [large;0;0],xa(:,j),xc(:,i));
        I = I + vfil(xb(:,j),xb(:,j) + [large;0;0],xc(:,i));
        A(i,j) = I(1)*n(1,i) + I(2)*n(2,i) + I(3)*n(3,i);
    end
    rhs(i) = -(Q(1)*n(1,i) + Q(2)*n(2,i) + Q(3)*n(3,i));
end
gamma = A\rhs';

% Forces at centres of bound vortices
bc(:,:) = 0.5*(xa(:,:) + xb(:,:));
for i = 1:N
    % first find the local velocity vector u on each load element i
    u = Q;
    for j = 1:N
        u = u + vfil(xa(:,j),xb(:,j),bc(:,i))*gamma(j);
        u = u + vfil(xa(:,j) + [large;0;0],xa(:,j),bc(:,i))*gamma(j);
        u = u + vfil(xb(:,j),xb(:,j) + [large;0;0],bc(:,i))*gamma(j);
    end
    % u cross s gives the direction of the force
    s = xb(:,i)-xa(:,i);
    Fx(i) = (u(2)*s(3)-u(3)*s(2))*gamma(i);
    Fz(i) = (u(1)*s(2)-u(2)*s(1))*gamma(i);
end

% convert to lift and drag coefficients
Cl = (sum(Fz(1:N))*cos(alpha)-sum(Fx(1:N))*sin(alpha))/(0.5*bw*cw);
```

Program 2. Example of the N-element horseshoe vortex method to rectangular wings.

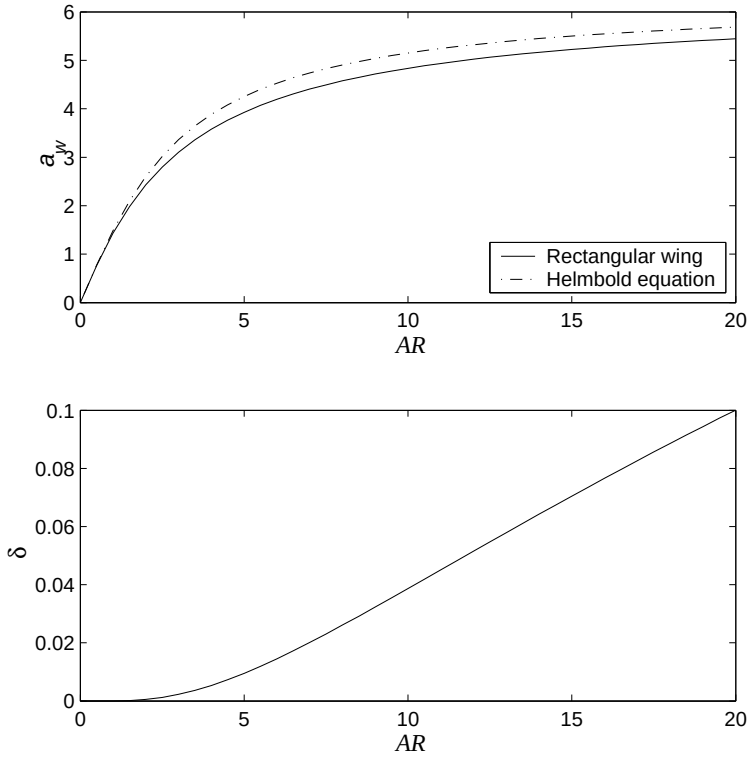

Figure 9. Effect of aspect ratio on the lift slope $a_W = \mathrm{d}C_L/\mathrm{d}\alpha$ (upper plot) and induced drag factor $\delta = C_{D_i}\pi AR/C_L^2 - 1$ (lower plot) of rectangular wings, computed with 100 horseshoe elements across a full wing span.

4. Aerodynamics of wings

The basic wing program of the previous section can be easily extended to cover effects of taper, sweep, dihedral, twist and ground proximity. In this section we explain how the basic problem needs to be modified and review some of the main results. In each case the wing is assumed to be symmetric about the x-z plane, and the equations are defined for the starboard wing only. In fact the program used to generate all the results in this section used the symmetry of the wing to reduce the size of the matrix by a factor of two. All the computations were done with 50 horseshoe elements across a wing semi-span.

4.1 *Effect of taper*

The chord variation of a straight tapered wing is given by

$$c(y) = c_{root} + \frac{2y}{b}\left(c_{tip} - c_{root}\right)$$

Defining $\sigma = c_{tip}/c_{root}$ as a taper ratio and setting the mean chord to unity, we can write

$$c_{root} = \frac{2}{1+\sigma}$$

and

$$c_{tip} = \frac{2\sigma}{1+\sigma}$$

Taper is used in practice to reduce the induced drag down to levels comparable with elliptic planforms without the manufacturing difficulties associated with the latter. Figure 10 plots δ defined by (11) (which would be equal to one for elliptic wings) against taper ratio for wings with various aspect

ratios. It can be seen that there exists an optimum taper ratio, close to $\sigma = 0.4$ for wings of high aspect ratio. To decide the optimum values of aspect ratio and taper ratio for aircraft applications it is necessary to consider the wing structural design and aircraft performance, in addition to the aerodynamics.

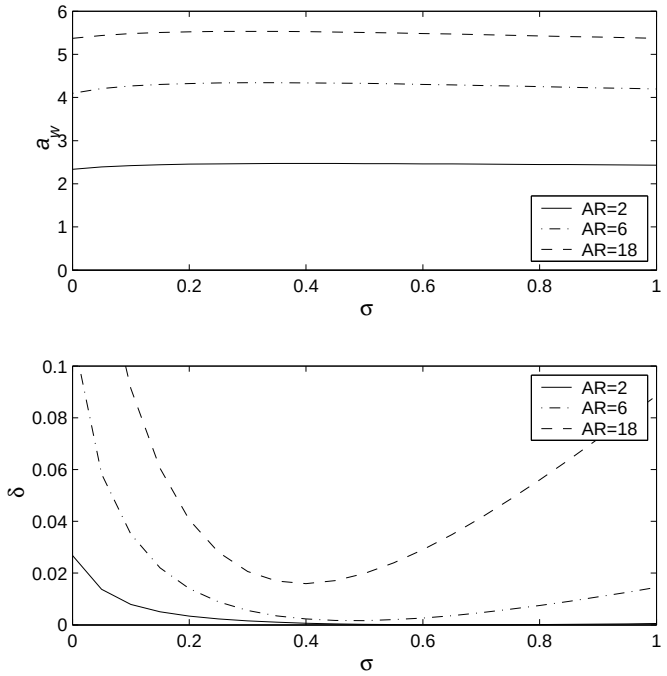

Figure 10. Effect of taper ratio on lift slope $a_W = \mathrm{d}C_L/\mathrm{d}\alpha$ (top) and induced drag factor $\delta = C_{D_i}\pi AR/C_L^2 - 1$ (bottom).

4.2 *Effect of twist*

Wing twist is another method of redistributing the lift across the span. If we define the wing incidence at the wing root we can account for twist by adjusting the normal vector n at the control points across the span. We make no distinction between geometric twist (physically twisting the wing) and aerodynamic twist (varying the zero lift angle of the section across the span) and define γ as the twist angle of the zero lift line (positive for nose up twist). Hence the unit normal vector at the control point is changed to $\mathbf{n}_i = [\sin\gamma; 0; \cos\gamma]$ and the control points themselves are rotated by γ around the aerodynamic centre. Using a linear twist variation on a tapered wing with $AR = 6$ at $\alpha = 5^\circ$, Figure 11 shows the effect on the induced drag factor δ. It can be seen that twist can be used in combination with taper to modify the induced drag performance. However, a common application of twist is not related to optimum cruise performance, but to improve stall behaviour of wings, especially of swept wings. It is important to avoid the outboard parts of a wing stalling first, as this can lead to large rolling moments, potentially sending an aircraft out of control. If this is a possibility the wing tips are twisted nose down (termed 'washout') to reduce the incidence and ensure that the root stalls first.

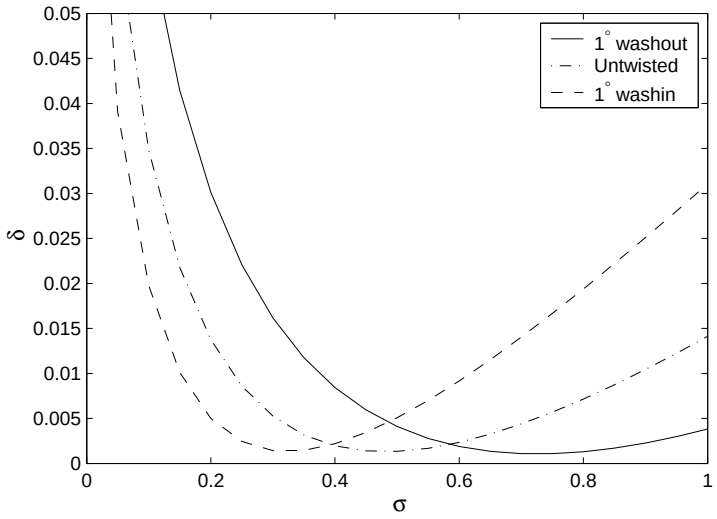

Figure 11. Effect of wing twist on induced drag factor as a function of taper ratio.

4.3 *Effect of sweep*

Sweep is used to delay the appearance of severe compressibility effects, manifested as a drag rise at transonic Mach numbers. For example simple compressible flow theory shows that a wing with a sweep angle $\Lambda = 40^\circ$ operating at Mach 0.85, actually 'sees' a local Mach number of $M\cos\Lambda = 0.65$. Here, we only consider the low-speed performance of such wings. The sweep is introduced simply by sweeping the quarter chord line (Figure 12), so the increments in horseshoe vortex A and B locations are $\Delta x = \Delta y \tan\Lambda$.

Figure 13 shows the effect of sweep angle on the lift slope a_w and (lower plot) the induced drag factor δ of a rectangular wing. Sweep is seen to reduce the lift slope and worsen the induced drag. Thus there is a price to be paid for high speed flight with delayed onset of the transonic drag rise, in that the wings must operate at a higher incidence compared to an unswept wing for the same lift coefficient, and will require either greater wing area or better high-lift devices in order to maintain the same $C_{L,\max}$ and hence the minimum flight speed for landing. From Figure 13 we see that forward and backward sweep have a similar effect on the lift slope, but that the induced drag is worse on aft-sewpt wings than on forward swept wings. There is also a difference in lift distribution, with forward-swept wings having a lower root bending moment. For conventional wing structures, however, these advantages of forward-swept wings are overridden by structural dynamic considerations.

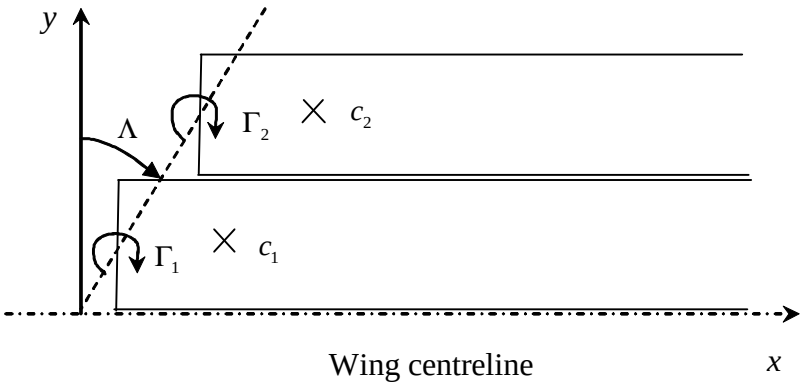

Figure 12. Incorporation of sweep angle into the horseshoe vortex geometry.

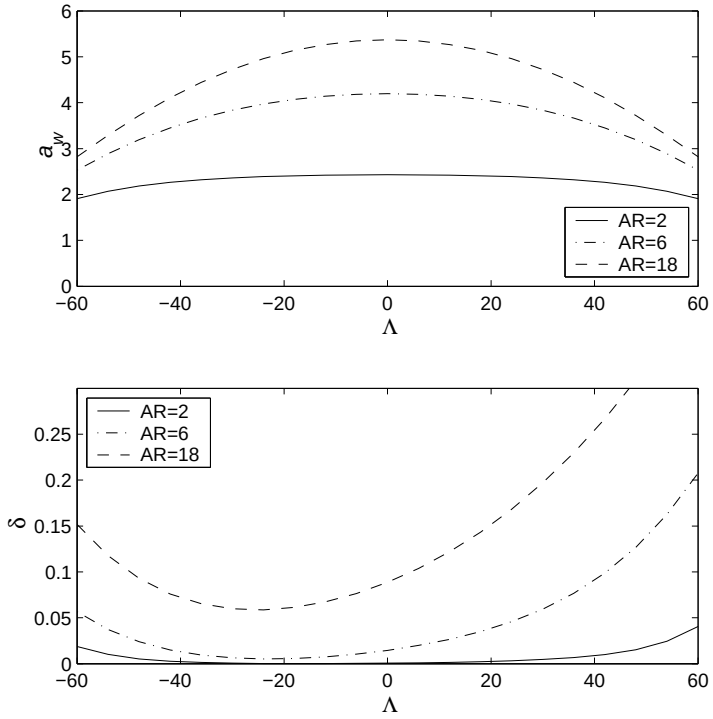

Figure 13. Effect of sweep angle on the lift slope $a_W = \mathrm{d}C_L/\mathrm{d}\alpha$ (top) and induced drag factor $\delta = C_{D_i}\pi AR/C_L^2 - 1$ (bottom) of a rectangular wing.

4.4 *Effect of dihedral*

The dihedral angle Γ is defined on Figure 14 as the angle the starboard wing is turned upward relative to the horizontal. A negative dihedral angle is known as anhedral.

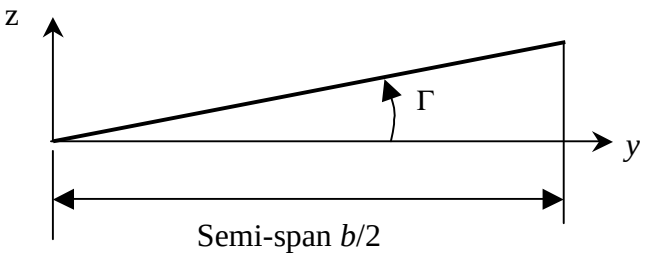

Figure 14. Definition of the dihedral angle.

To add this effect into the code we need to rotate the normal vector, so that (on the starboard wing) $\mathbf{n}_i = \left[0; -\sin(\Gamma); \cos(\Gamma)\right]$ and include steps of $\Delta z = \Delta y \tan\Gamma$ in the locations of the A and B points of the horseshoe elements. Figure 15 shows the effect of dihedral on the lift slope and induced drag factor. Note that we have kept the winspan and wing planform area fixed, so the wing wetted area (and hence structural weight) increases as dihedral is added. The reduction in induced drag factor is not therefore of practical use.

The main reason for adding dihedral is to improve the lateral stability of an aircraft, especially if the wings are mounted below the fuselage centreline.

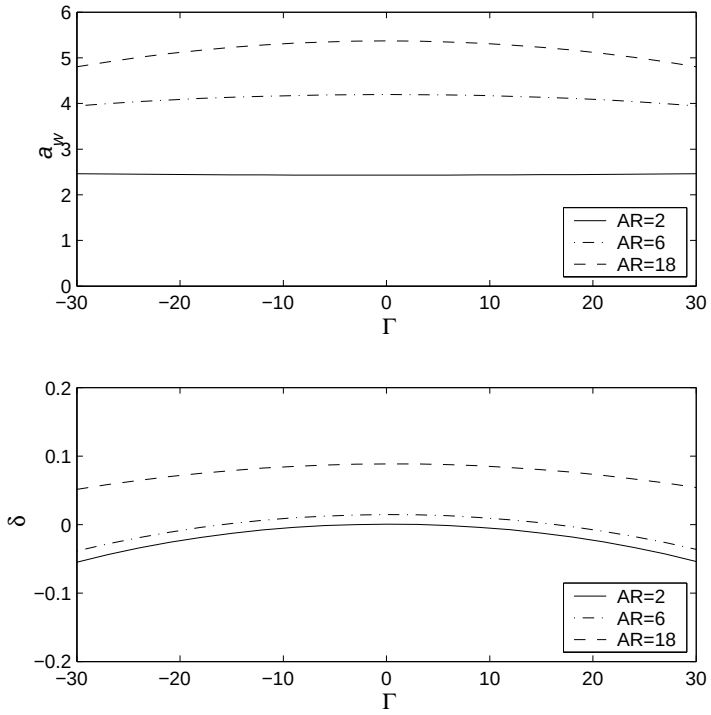

Figure 15 Effect of dihedral angle on lift slope and induced drag factor.

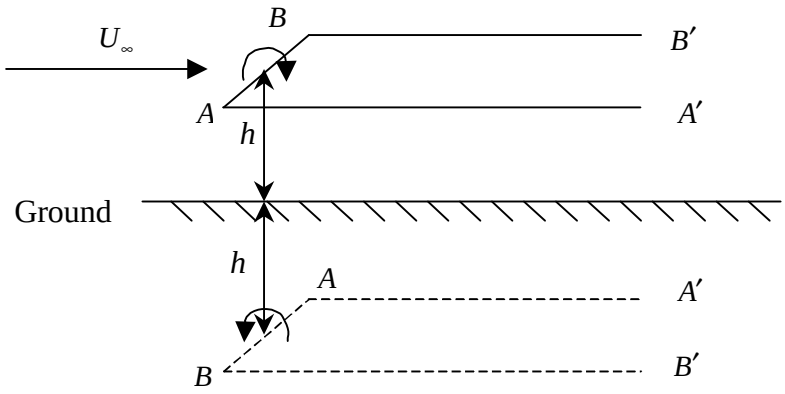

Figure 16. Modelling the effect of the ground. Note that the ordering of points around the reflected horseshoe is reversed to allow for the reverse circulation.

4.5 *Ground effect*

To model a lifting surface a distance h above the ground we must have an image horseshoe vortex system located at $-h$. The image must have the opposite sign of circulation to ensure that the ground is a streamline of the resultant flow. For a single horseshoe vortex the situation is shown on Figure 16.

The reflection is easily accomplished by multiplying the z-components by -1. Three extra calls to the function *vfil* are needed to account for the image horseshoe, but otherwise the procedure is exactly the same. Figures 17 shows lift slope and induced drag factor as functions of height h for wings of various aspect ratio. Note that one limitation of this model is that we have taken the horseshoe model parallel to the ground and the freestream velocity inclined at the angle of incidence. It would be more reasonable to take the freestream velocity parallel to the ground, and use a cranked horseshoe model

with the first part of the horseshoe (for example up to some point downstream of the trailing edge) inclined at the angle of incidence but the remainder of the trailing vortices parallel to the ground.

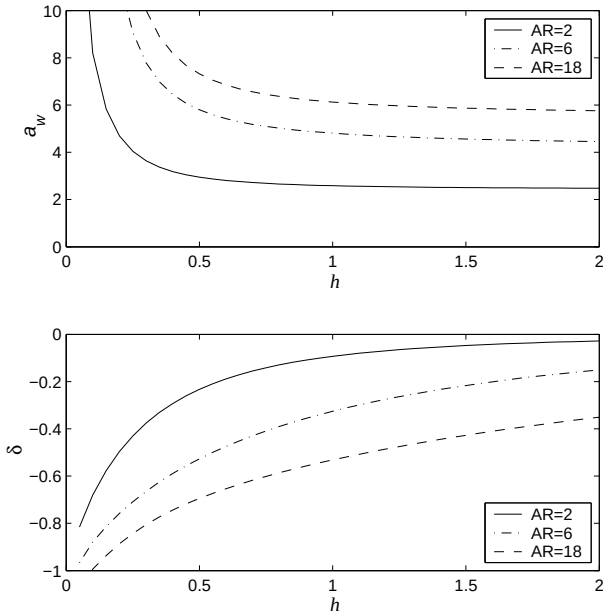

Figure 17 Effect of ground proximity

Appendix 1. Theoretical basis for equation (1)

For potential flow we can define a divergence-free vector potential **B** such that the velocity vector **q** is given by $\mathbf{q} = \nabla \times \mathbf{B}$. The vorticity vector $\boldsymbol{\omega}$ is the curl of the velocity and using a standard vector identity we have

$$\boldsymbol{\omega} = \nabla \times \mathbf{q} = \nabla \times (\nabla \times \mathbf{B}) = \nabla (\nabla . \mathbf{B}) - \nabla^2 \mathbf{B}$$

Since **B** is divergence free the governing equation for **B** is

$$\nabla^2 \mathbf{B} = -\boldsymbol{\omega} \tag{A1.1}$$

Using Green's method we can solve this for any distribution of vorticity in space, giving

$$\mathbf{B} = \int_V \frac{\boldsymbol{\omega}}{4\pi r} \mathrm{d}V$$

where *r* is distance from each part of the vorticity field to the observer position. The velocity is given by the curl of this (keeping vorticity fixed during the differentiation):

$$\mathbf{q} = \frac{1}{4\pi} \int_V \nabla \times \left(\frac{\boldsymbol{\omega}}{r} \right) \mathrm{d}V = \frac{1}{4\pi} \int_V \frac{\boldsymbol{\omega} \times \mathbf{r}}{r^3} \mathrm{d}V$$

For a vortex filament we can replace $\boldsymbol{\omega} \mathrm{d}V$ with $\Gamma \mathrm{d}\mathbf{l}$, where Γ is the circulation and d**l** is a vector locally tangential to the vortex filament. Thus we have derived the Biot-Savart law:

$$\boxed{\mathbf{q} = \frac{\Gamma}{4\pi} \int \frac{\mathrm{d}\mathbf{l} \times \mathbf{r}}{r^3}} \tag{A1.2}$$

In the 2D plane formed by a straight line vortex filament and an observer point *C* we can find the magnitude of the velocity $q = |\mathbf{q}|$ due to the filament as

$$q = \frac{\Gamma}{4\pi} \int_A^B \frac{\sin\theta}{r^2} \mathrm{d}l \tag{A1.3}$$

where the angle θ is defined on Figure A.1 and we have used $|\mathrm{d}\mathbf{l} \times \mathbf{r}| = |\mathrm{d}\mathbf{l}||\mathbf{r}| \sin\theta$. Note that the origin of the *l* axis is the point where *h* intersects the line *AB*. We can see that $r^2 = h^2 / \sin^2\theta$, $l = -h/\tan\theta$ and hence $\mathrm{d}l/\mathrm{d}\theta = h/\sin^2\theta$. Substitution into (A1.3) gives the final result

$$\boxed{q = \frac{\Gamma}{4\pi h} \int_{\theta_A}^{\theta_B} \sin\theta \mathrm{d}\theta = \frac{\Gamma}{4\pi h} (\cos\theta_A - \cos\theta_B)} \tag{A1.4}$$

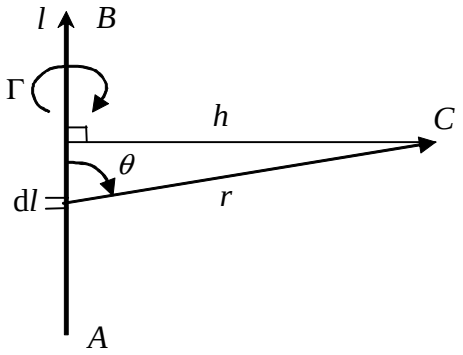

Figure A.1 Diagram defining the geometry for integration of the Biot-Savart law for a straight line segment *AB*.

Appendix 2. Lifting line theory.

A2.1 *Downwash angle*

In lifting line theory the circulation is treated as a continuous function of the spanwise variable *y* such that the local strength of the trailing vortex sheet is $(\mathrm{d}\Gamma/\mathrm{d}y)\mathrm{d}y$. Using (1) and integrating across the span, the downwash velocity at any spanwise position y_0 is given by

$$\alpha_i = \frac{1}{4\pi U_\infty}\int_{-b/2}^{b/2}\frac{(\mathrm{d}\Gamma/\mathrm{d}y)}{y_0 - y}\mathrm{d}y$$

We make a change of variables using $y = -\frac{1}{2}b\cos\theta$ and assume that the circulation can be represented by a Fourier series

$$\Gamma = 2bU_\infty\sum_n A_n \sin n\theta \tag{A2.1}$$

Thus the downwash angle (induced angle of attack) is given by

$$\alpha_i = \frac{1}{\pi}\int_0^\pi \frac{\sum nA_n\cos n\theta}{\cos\theta - \cos\theta_0}\mathrm{d}\theta$$

For each element in the summation the integral can be carried out using Glauert's integral

$$\int_0^\pi \frac{\cos n\theta}{\cos\theta - \cos\theta_0}\mathrm{d}\theta = \frac{\pi\sin n\theta_0}{\sin\theta_0}$$

and so the downwash angle simplifies to

$$\boxed{\alpha_i = \sum nA_n\frac{\sin n\theta_0}{\sin\theta_0}} \tag{A2.2}$$

A2.2 *Aerodynamic coefficients*

The lift coefficient is obtained by integrating the circulation distribution

$$C_L = \frac{2}{U_\infty S_w}\int_{-b/2}^{b/2}\Gamma\mathrm{d}y = 2AR\int_0^\pi\sum A_n\sin n\theta\sin\theta\mathrm{d}\theta \tag{A2.3}$$

To simplify this we use the orthogonality of the sine function:

$$\int_0^\pi \sin m\theta\sin n\theta\mathrm{d}\theta = 0 \quad \text{for } m \neq n$$
$$= \pi/2 \text{ for } m = n \tag{A2.4}$$

We only get terms in A2.3 when $n = 1$, when the integral is $\pi/2$. Thus

$$\boxed{C_L = \pi AR\,A_1} \tag{A2.5}$$

In a similar fashion we can get the drag coefficient (see Figure 4 and related discussion) as

$$C_{D_i} = \frac{2}{U_\infty S_w}\int_{-b/2}^{b/2}\alpha_i\Gamma\mathrm{d}y = 2AR\int_0^\pi \Sigma\left(A_m\sin m\theta\right)\Sigma\left(nA_n\sin n\theta\right)\mathrm{d}\theta$$

The time we only get terms when $n = m$, leaving

$$C_{D_i} = \pi AR\sum nA_n^2$$

or, splitting off the first coefficient and using the lift coefficient from (A2.5)

$$\boxed{C_{D_i} = \frac{C_L^2}{\pi AR}\left(1 + \frac{1}{A_1^2}\sum_{n=2}^{N} nA_n^2\right)} \qquad \text{(A2.6)}$$

A2.3 *Minimum induced drag and elliptic planforms*

Since the term in brackets contains a sum of squared terms, it has a lowest possible value of one and we see that the *minimum* induced drag is

$$\boxed{C_{D_i \min} = C_L^2 / \pi AR} \qquad \text{(A2.7)}$$

This occurs when all the higher ($n \geq 2$) Fourier coefficients are zero. This leaves the circulation given by just the first term in the series, i.e.

$$\Gamma = 2bU_\infty A_1 \sin\theta \qquad \text{(A2.8)}$$

and we can note from A2.2 that the downwash angle is constant across the span. Now we can specify the local section lift coefficient to be 2π times the local incidence (the aircraft incidence less the downwash angle)

$$\boxed{C_L = \frac{2\Gamma}{U_\infty c} = 2\pi\left(\alpha - \alpha_i\right)} \qquad \text{(A2.9)}$$

For constant α across the span (an untwisted wing) the right hand side is a constant and we must have

$$c = c_0 \sin\theta = c_0\sqrt{1 - \left(\frac{2y}{b}\right)^2} \qquad \text{(A2.10)}$$

where c_0 is the root chord. This is the equation for an ellipse, so the minimum induced drag condition of a planar wing can be produced by an elliptic untwisted unswept planform. The mean chord is $\bar{c} = c_0\pi/4$ and substitution of (A2.8) and (A2.10) into (A2.9) lets us finally evaluate the first Fourier coefficient as

$$A_1 = \frac{2\alpha}{2 + AR}$$

Hence from (A2.5) the lift slope of an elliptic wing is

$$\boxed{a_w = \frac{2\pi}{1 + \frac{2}{AR}}} \qquad \text{(A2.11)}$$

What does lifting line theory tells us that is additional to the single element horseshoe vortex model of section 2? Firstly it tells us that the result for drag given by (8) and lift slope at high aspect ratios are appropriate for wings with an elliptic distribution of circulation. Secondly it tells us that the elliptic result is the best that can be done for planar wings. In terms of actual predictions the single-element model is preferred since it merges cleanly into the slender wing results. (Note that (A2.11) gives an incorrect result of $a_w = \pi AR$ for slender wings).

By using the horseshoe vortex as a basic element, the results of section 3 are better than standard lifting line theory. In fact they correspond more closely to the 'extended' lifting line approach of Weissinger (discussed in Schlichting & Truckenbrodt, 'Aerodynamics of the Airplane, McGraw-Hill 1971), which also applies tangential flow to the three-quarter chord position.